Sedimentology (1995) **42**, 491–513

Mean flow and turbulence structure over fixed, two-dimensional dunes: implications for sediment transport and bedform stability

S. J. BENNETT and J. L. BEST
Department of Earth Sciences, University of Leeds, Leeds LS2 9JT, West Yorkshire, UK

ABSTRACT

Detailed measurements of flow velocity and its turbulent fluctuation were obtained over fixed, two-dimensional dunes in a laboratory channel. Laser Doppler anemometry was used to measure the downstream and vertical components of velocity at more than 1800 points over one dune wavelength. The density of the sampling grid allowed construction of a unique set of contour maps for all mean flow and turbulence parameters, which are assessed using higher moment measures and quadrant analysis. These flow field maps illustrate that: (1) the time-averaged downstream and vertical velocities agree well with previous studies of quasi-equilibrium flow over fixed and mobile bedforms and show a remarkable symmetry from crest to crest; (2) the maximum root-mean-square (RMS) of the downstream velocity values occur at and just downstream of flow reattachment and within the flow separation cell; (3) the maximum vertical RMS values occur within and above the zone of flow separation along the shear layer and this zone advects and diffuses downstream, extending almost to the next crest; (4) positive downstream skewness values occur within the separation cell, whereas positive vertical skewness values are restricted to the shear layer; (5) the highest Reynolds stresses are located within the zone of flow separation and along the shear layer; (6) high-magnitude, high-frequency quadrant-2 events ('ejections') are concentrated along the shear layer (Kelvin–Helmholtz instabilities) and dominate the contribution to the local Reynolds stress; and (7) high-magnitude, high-frequency quadrant-4 events occur bounding the separation zone, near reattachment and close to the dune crest, and are significant contributors to the local Reynolds stress at each location. These data demonstrate that the turbulence structure associated with dunes is controlled intrinsically by the formation, magnitude and downstream extent of the flow separation zone and resultant shear layer. Furthermore, the origin of dune-related macroturbulence lies in the dynamics of the shear layer rather than classical turbulent boundary layer bursting. The fluid dynamic distinction between dunes and ripples is reasoned to be linked to the velocity differential across the shear layer and hence the magnitude of the Kelvin–Helmholtz instabilities, which are both greater for dunes than ripples. These instabilities control the local flow and turbulence structure and dictate the modes of sediment entrainment and their transport rates.

INTRODUCTION

Dunes are one of the most common bedforms generated in unidirectional aqueous flows and are often responsible for both the majority of bedload transport and flow resistance as well as being a dominant sedimentary structure in many fluvial sequences. Dunes can form in a wide range

Table 1. Summary of past research on flow over fixed bedforms in unidirectional water flows.

	Bedform morphology							Flow conditions								
Source	Composition	Set	Wave-length, (λ), m	Height (h), m	Leeside angle	λ/Y	Y/h	Width (W)	Depth (Y)	Mean down-stream velocity ($\bar{U}$), m s^{-1}	u'	v'	Flow measurement techniques	No. of profiles	No. of points/ profile	Data rate (Hz)	Notes
Vanoni & Nomicos (1960)	chemically stabilized 0·091 mm sand	I(2)	*c.* 0·11	*c.* 0·022	na	1·26	3·95	0·267	0·087	0·375	no	no	pitot tube	1	8	—	(1)
Raudkivi (1963)	smooth metal sheet	—	0·386	0·025 (0·022)	*c.* 29°	3·06	3·04 (3·45)	0·076	0·126	0·299	no	no	pitot tube; pressure taps	*c.* 2	19–20	—	(1), (2)
Raudkivi (1966)	smooth metal sheet	—	0·386	0·025	*c.* 29°	3·06	3·04	0·076	0·126	0·299	yes	yes	pitot tube; constant temperature anemometer	4	7–10	na	(3)
Vanoni & Hwang (1967)	chemically stabilized 0·23 mm sand	9–14 9–15	0·162 0·168	0·016 0·015	*c.* 26° *c.* 26°	2·31 2·30	3·38 4·87	0·267 0·267	0·070 0·073	0·228 0·381	no	no	pitot tube; pressure taps	14–18	6–13	—	(1), (2)
Rifai & Smith (1971)	smooth brass	—	0·51	0·051	30°	1·67 (1·83)	5·98 (5·45)	0·381	0·305 (0·278)	0·576	yes	no	constant temperature anemometer	4	6–19	625	(3); see also Rifai & Smith (1969)
McCorquodale & Giratalla (1973)	perspex roughened with 0·2 mm sand	a	0·064	0·0048	90°	0·50	26·68	0·127	0·127	0·229	yes	yes	constant temperature anemometer; pitot tube	1	6	na	(3)
	mortar cast from Plaster of Paris ripple mould	b	0·089	0·0106	*c.* 30°	0·70	11·98	0·127	0·127	0·229	yes	yes		1	8	na	
Vittal, Ranga Raju & Garde (1977)	plywood smooth and roughened with 0·6 mm sand	— — — —	0·600 0·450 0·306 0·015	0·03 0·03 0·03 0·03	30° 30° 30° 30°	1·000 0·750 0·510 0·025	20 20 20 20	na	0·600	na	no	no	pitot tube & pressure taps	3	5–10	—	(2)
Itakura & Kishi (1980)	cement roughened with 0·42 mm sand	—	0·30	0·015	*c.* 30°	4·7	4·3	0·10	0·064	*c.* 0·32	no	yes	constant temperature anemometer	5	4	100	(3)

Fehlman (1985)	smooth plastic	I	0·915	0·137	30°	4·14–2·83	1·61–2·36	0·61	0·221–0·323	0·147–0·653	no	no	total force measuring device; pitot tube	—	—	—	(2); see also Mendoza & Shen (1990); Shen *et al.* (1990)
	plastic roughened with 1·75 mm sand	II	0·915	0·137	30°	4·14–2·83	1·61–2·36	0·61	0·221–0·323	0·147–0·534							
Van Mierlo & de Ruiter (1988)	concrete roughened with 1·5 mm sand	T5	1·6	0·08	*c.* 28°	6·35	3·15	1·5	0·252	0·394	yes	yes	LDA; bed pressure transducers	10	12–22	na	(2), (3); see also van der Knapp *et al.* (1991); John *et al.* (1993); Lyn (1993)
		T6	1·6	0·08	*c.* 28°	4·79	4·18	1·5	0·334	0·513							
Nelson & Smith (1989a)	concrete roughened with fine sand	—	0·8	0·04	30°	4	5	0·70	0·20	0·50	yes	no	LDA	16	30–54	>256**	(3)
Wiberg & Nelson (1992)	concrete roughened with 0·25 mm sand	sym	0·16	0·02	30°	0·73	11	0·70	0·22	0·38	yes	yes	LDA	6	21–35	500–2000**	(3)
		asym	0·16	0·02	30°	1·33	6	0·70	0·12	0·43							
						0·73	11		0·22	0·40							
Lyn (1993)	wood roughened with 0·25 mm sand	2	0·15	0·012	45°	2·46	5·08	0·267	0·061	0·269	yes	yes	LDA	4	11–35	15–>60	(3)
		3	0·15	0·012	45°	2·46	5·08	0·267	0·061	0·551							
Nelson, McLean & Wolfe (1993)	concrete roughened with fine sand	—	0·16	0·02	30°	0·82–0·73	9·75–11·00	0·70	0·195–0·220	0·32–0·51	yes	yes	LDA	6	20–50	>256**	(3)
			0·80	0·04	30°	6·66–3·64	3·00–5·50	0·70	0·120–0·220	0·40–0·43							
McLean, Nelson & Wolfe (1994)	concrete roughened with fine sand	1	0·80	0·04	30°	3·81	5·25	0·90	0·210	0·482	yes	yes	LDA; acoustic profiler	15	*c.* 30	0·4–4	(3)
		2	0·80	0·04	30°	5·06	3·95	0·90	0·158	0·377							
		3	0·80	0·04	30°	1·47	13·65	0·90	0·546	0·284							
This study	concrete roughened with 0·22 mm glass spheres	—	0·63	0·04	30°	6·3	2·5	0·30	0·10*	0·57*	yes	yes	LDA	76	20–30	20–100	(3); see also Bennett & Best (1995)

*Over bedform crest; **number of particles measured (no time-scale given). (1) Vertical velocity profiles; (2) bed shear and fluid pressure; (3) vertical velocity and turbulence profiles.

of sediment sizes and grades, from well-sorted fine to coarse sands (see Guy *et al.*, 1966; Williams, 1967; Costello, 1974; Nordin & Rundquist, 1975; Allen, 1982) to poorly sorted gravels (Hubbell *et al.*, 1987; Dinehart, 1989, 1992), suggesting common formative processes across a wide range of grain roughnesses (Best, 1995). Dune morphology may also change rapidly and undergo complex processes of growth, attenuation and destruction (Gabel, 1993).

Fluid flow over dunes is well known and can be subdivided into five major zones: (1) accelerated, converging flow over the dune crest; (2) a zone of flow separation on the crest lee-side with its characteristic recirculation pattern; (3) a decelerated wake region overlying the separation cell and extending downsteam; (4) an outer, near-surface region overlying this wake; and (5) the downstream growth of a new, internal boundary layer originating at reattachment (see Raudkivi, 1966; Engelund & Fredsøe, 1982; Müller & Gyr, 1982, 1986; McLean & Smith, 1986; and many others). Above the separation cell and along the free-shear layer associated with this zone, high turbulence intensities and Reynolds stresses are observed (Raudkivi, 1966; Rifai & Smith, 1971; Engelund & Fredsøe, 1982; Müller & Gyr, 1982, 1986; McLean & Smith, 1986; Mendoza & Shen, 1990; Nelson *et al.*, 1993; McLean *et al.*, 1994). This wake region diffuses both vertically and horizontally from the point of flow separation, growing larger in size but decreasing in turbulent energy. The new internal boundary layer interacts with this wake zone and the two effectively merge by the next dune crest, approximating uniform boundary layer conditions (McLean *et al.*, 1994). Recognition of these dune characteristics has facilitated: (1) the development of numerical models of flow over dunes (McLean & Smith, 1986; Nelson & Smith, 1989a; Mendoza & Shen, 1990; Johns *et al.*, 1990, 1993); and (2) the quantitative partitioning of the total boundary shear stress into components of skin friction and form drag (e.g. Smith & McLean, 1977; Nelson & Smith, 1989b, Wiberg & Nelson, 1992). However, despite many studies of flow over dunes (Table 1), there has been little integration of this information into theories for bedform stability and the mechanics of sediment transport.

Several studies have suggested that macroturbulence associated with dune bedforms is important in both the entrainment and transport of sediment and in controlling the formation and hydraulic stability of dunes. Experimental and field investigations of dunes have documented turbulent events called 'kolks' or 'boils' (Matthes, 1947; Coleman, 1969; Jackson, 1976; Itakura & Kishi, 1980; Nezu *et al.*, 1980). Boils have long been suggested to be the surface manifestation of slowly rotating, upward-tilting vortices whose origin is near the bed (Matthes, 1947). Several recent field studies have quantified the high suspended sediment concentrations associated with these events (e.g. Rood & Hickin, 1989; Lapointe, 1992; Kostaschuk & Church, 1993). Jackson (1976) derived empirically the dimensionless periodicity of boils associated with dunes (T_b) of the form:

$$T_b = T\bar{U}/Y \sim 3\text{–}7 \quad (1)$$

where T is the boil period, $\bar{U}$ is mean downstream velocity and Y is flow depth. Because the value in Eq. (1) is identical to the periodicity of 'burst' events within turbulent boundary layers (e.g. Rao *et al.*, 1971), both Jackson (1976) and Yalin (1977, 1992) reasoned that the source of these boils, and hence the origin of dunes, must be related to these boundary layer events. Despite their widespread recognition, the location and mechanism of boil development still remains poorly understood (see discussion in Nezu & Nakagawa, 1993).

Recent work, however, has suggested that dune-related macroturbulence is more likely to be associated with Kelvin–Helmholtz instabilities shed off the separation-zone shear layer (Müller & Gyr, 1982, 1986; Rood & Hickin, 1989; see also Lane, 1944; Korchokha, 1968). These turbulent events do not share a common origin to boundary layer bursting, although they may be indistinguishable in a velocity time–series record. Levi (1983, 1991) suggested such dune-related macroturbulence is due to eddy shedding, where the frequency of shedding, f, can be determined from the Strouhal relationship:

$$St = fY/\bar{U} \sim 0{\cdot}16 \quad (2)$$

where St is the Strouhal number, Y is the upstream depth before separation and $\bar{U}$ is the mean downstream approach velocity (Levi, 1983, 1991). However, no detailed information has been collected to quantify eddy shedding over dunes nor how this shedding may be related to sediment transport mechanisms and dune stability. Furthermore, eddy shedding is only one kind of turbulent event, and other fluid motions (e.g. 'sweeps') may be equally influential in controlling sediment transport and dune formation.

The generation and hydraulic stability of dunes has been described through linear stability analysis (e.g. Kennedy, 1963, 1969; Hayashi, 1970; Smith, 1970; Richards, 1980; Engelund & Fredsøe,

1982). In this analysis, the equations for motion of both fluid and sediment are linearized and flow over an infinitesimally small bed perturbation is investigated in order to determine the response of the perturbation to the flow, thus predicting stable or unstable bed waves (see McLean, 1990, p. 133). Critical to this analysis is the determination of the phase difference of the sediment transport rate relative to the bed topography. Stated simply, the maximum fluid stress occurs upstream of the perturbation crest and, assuming sediment transport is a function of the local stress, deposition occurs at the crest and produces bedform growth. This analysis, however, ignores the interactions between sediment transport and bed topography with the turbulent flow field, especially the occurrence and downstream extent of flow separation, the development of a shear layer and the frequent, large, energetic fluid motions (macroturbulence) that are dependent on bedform morphology and position. In order to understand more fully the mechanics of bedforms and their hydraulic stability, a detailed examination of the fluid dynamics over fully mobilized, hydraulically stable equilibrium bedforms is required to assess these complex fluid–bed–grain interactions.

As a first step in this process, the aim of the present study was to obtain highly detailed experimental data on the mean flow and turbulence fields over fixed, two-dimensional dunes in order to: (1) investigate and document the origins of dune-related macroturbulence; and (2) use these results to shed light upon the mechanisms of sediment transport and the origin of dunes, and thereby provide some insight into the fluid dynamic differentiation of dunes and ripples. Our sampling strategy enabled the construction of uniquely detailed contour maps of the various flow and turbulence parameters over the entire flow field, thus avoiding the problems associated with an inadequate sample-grid resolution.

EXPERIMENTAL METHODOLOGY

The experiments were conducted in the Sedimentological Fluid Dynamics Laboratory, Department of Earth Sciences, University of Leeds, using a recirculating flume 10 m long, 0·3 m wide and 0·3 m deep. Because bedform migration and three-dimensionality of form are removed from the experimental set-up, the use of fixed bedforms allows the acquisition of detailed, reproducible, time-averaged measurements of flow and turbulence. However, these artificial bedforms must be subjected to the typical flow conditions in which they are generated (Table 1). Using a wooden template, a series of two-dimensional concrete bedforms were moulded from typical profiles of equilibrium 'maximum steepness' dunes observed by Bridge & Best (1988) generated in 0·3 mm diameter sand. A total of seven bedforms, each having a length of 0·63 m, a height of 0·04 m and a slip-face angle of 30°, were cast. The surfaces of these bedforms were painted and covered with glass spheres, 0·22 mm in diameter, whilst the paint was still wet, producing a surface with the appropriate grain roughness. The present experiment maintained the ratios of bedform-wavelength : flow-depth (5·4), wavelength : bedform-height (15·75) and flow-depth : bedform-height (2·9) as described in Bridge & Best (1988) and commonly observed in other studies of dunes (see Allen, 1982). The conservation of such ratios used in conjunction with the appropriate velocity fields (see below) must be ensured so that the measurements obtained are typical of flow over fully developed bedforms (see Table 1).

The bedforms were placed in the flume and flow conditions identical to the mobile bed experiments of Bridge & Best (1988) were established (Table 2). Achievement of quasi-equilibrium flow over the fixed bedforms required adjustment of the pump discharge and flume slope while maintaining the correct mean flow velocity (see below) and water depth over successive bedform crests. This equilibration process was deemed complete when the appropriate mean flow velocity was achieved and the water depth over five consecutive dune crests was within ± 2 mm using sidewall-mounted scales (see McLean *et al.*, 1994, for a detailed discussion of the importance of establishing equilibrium flow over fixed bedforms).

At-a-point velocity and turbulence measurements were taken using a laser Doppler anemometer (LDA; for a general description of the principles of LDA see Buchhave *et al.*, 1979; Durst *et al.*, 1987). A DANTEC two-component fibre-optic LDA was used in backscatter mode with a 400 mm focal length lens and 100 mW argon-ion laser (using green light, λ_1=488 nm, for downstream (u) velocity and blue light, λ_1=514·5 nm, for the vertical (v) velocity). The LDA was operated with a 40 MHz frequency shift to enable the measurement of positive and negative flows along either axis. The LDA was run with a DANTEC Particle Dynamics Analyser processor, which operates on a correlation-type process (DANTEC, 1991), and signals were validated only

	Bridge & Best (1988)	This study
Flow depth (Y), m	0·10	0·10 (crest) 0·12 (stoss)
Mean velocity (U), m s^{-1}	*c.* 0·60	0·57 (crest) 0·49 (stoss)
Froude number (Fr)	0·61	0·58 (crest) 0·46 (stoss)
Mean shear velocity (U_*), m s^{-1}	0·062	0·041 U_{*B} 0·025 U_{*SF}
Dune wavelength, (λ), m	0·45–0·90	0·63
Dune height (h), m	0·025–0·04	0·04
h/λ	0·04 (mean)	0·063

Table 2. Summary of hydraulic conditions and bedform morphology used in this study and that of Bridge & Best (1988) on which the fixed dune morphology is based. Mean depth and velocities are given for the positions over the dune crest and a spatial average across the stoss slope. U_{*B} and U_{*SF} denote boundary and skin-friction shear velocities (see text).

when Doppler bursts of a sufficient threshold were recorded on both channels. The flow was seeded with 20 μm diameter titanium dioxide-coated mica flakes, which provide an excellent source of scattering centres, yielding data rates of between 20 and 100 Hz (normally 60 Hz) in this study. For the mean flow conditions used (see Table 2), sampling rates of approximately 60 to 70 Hz are desirable to ensure full characterization of the turbulence spectra (see Nezu & Nakagawa, 1993, p. 30). The probe head was mounted on a high-precision, electronically controlled traverse system which allowed the positioning of the laser intersection volume to within ± 0·1 mm.

Seventy-six vertical velocity profiles spaced 0·01 m apart were measured near the flume centreline over one bedform wavelength (Fig. 1b) with simultaneous downstream and vertical velocities being collected at 20 to 30 points within each profile. At each point, the flow was sampled for 60 s and a grid of over 1800 points was established (Fig. 1b), with the lowest point in each profile being 5 mm above the bed.

This LDA data was used to compute mean flow velocities (arithmetic particle averages) at each point and second and third moments of the velocity distributions defined as:

$$u' = \left[\frac{1}{n}\sum_{i=1}^{n}(u_i - \bar{U})^2\right]^{0.5} \quad (3)$$

$$v' = \left[\frac{1}{n}\sum_{i=1}^{n}(v_i - \bar{V})^2\right]^{0.5} \quad (4)$$

$$U_{skew} = \frac{1}{n}\sum_{i=1}^{n}\left[\frac{(u_i - \bar{U})}{u'}\right]^3 \quad (5)$$

$$V_{skew} = \frac{1}{n}\sum_{i=1}^{n}\left[\frac{(v_i - \bar{V})}{v'}\right]^3 \quad (6)$$

where u' and v' are the root-mean-square (RMS) values of the downstream and vertical components respectively, n is the number of observations, u_i and v_i are the instantaneous velocities, U and $\bar{V}$ are the time-averaged velocities at-a-point, and U_{skew} and V_{skew} are the skewness values of the velocity distribution. No attempt was made to correct for a velocity biasing effect (when the particle measuring rate is correlated to the magnitude of the instantaneous velocity vector in the flow; Adams & Eaton, 1988), because such bias is significant only in highly turbulent flows (i.e. velocities in excess of several metres per second; see also Gould & Loseke, 1993). The time-averaged local Reynolds stress at-a-point (τ_r) was determined using

$$\tau_r = -\rho\overline{uv} \quad (7a)$$

$$-\overline{uv} = \frac{1}{n}\sum_{i=1}^{n}(u_i - \bar{U})(v_i - \bar{V}) \quad (7b)$$

where ρ is fluid density.

This study also sought to examine the structure of turbulence over the dune bedform with respect to the type of turbulent event as defined through quadrant analysis. Quadrant analysis has been used to discriminate boundary layer turbulent events by examining the instantaneous deviations of velocity from the mean values (e.g. Lu & Willmarth, 1973; Bogard & Tiederman, 1986). Plotting the horizontal and vertical velocity fluctuations about a zero mean defines four quadrants (Fig. 2), with quadrant-2 and -4 events describing the 'ejection' and 'sweep' events of classical boundary layer studies and quadrants 1 and 3 defining 'outward' and 'inward' interactions. Each turbulent velocity pair may be investigated either through examination of the entire signal or only those events that lie above a certain threshold value (H; or hole size) defined as:

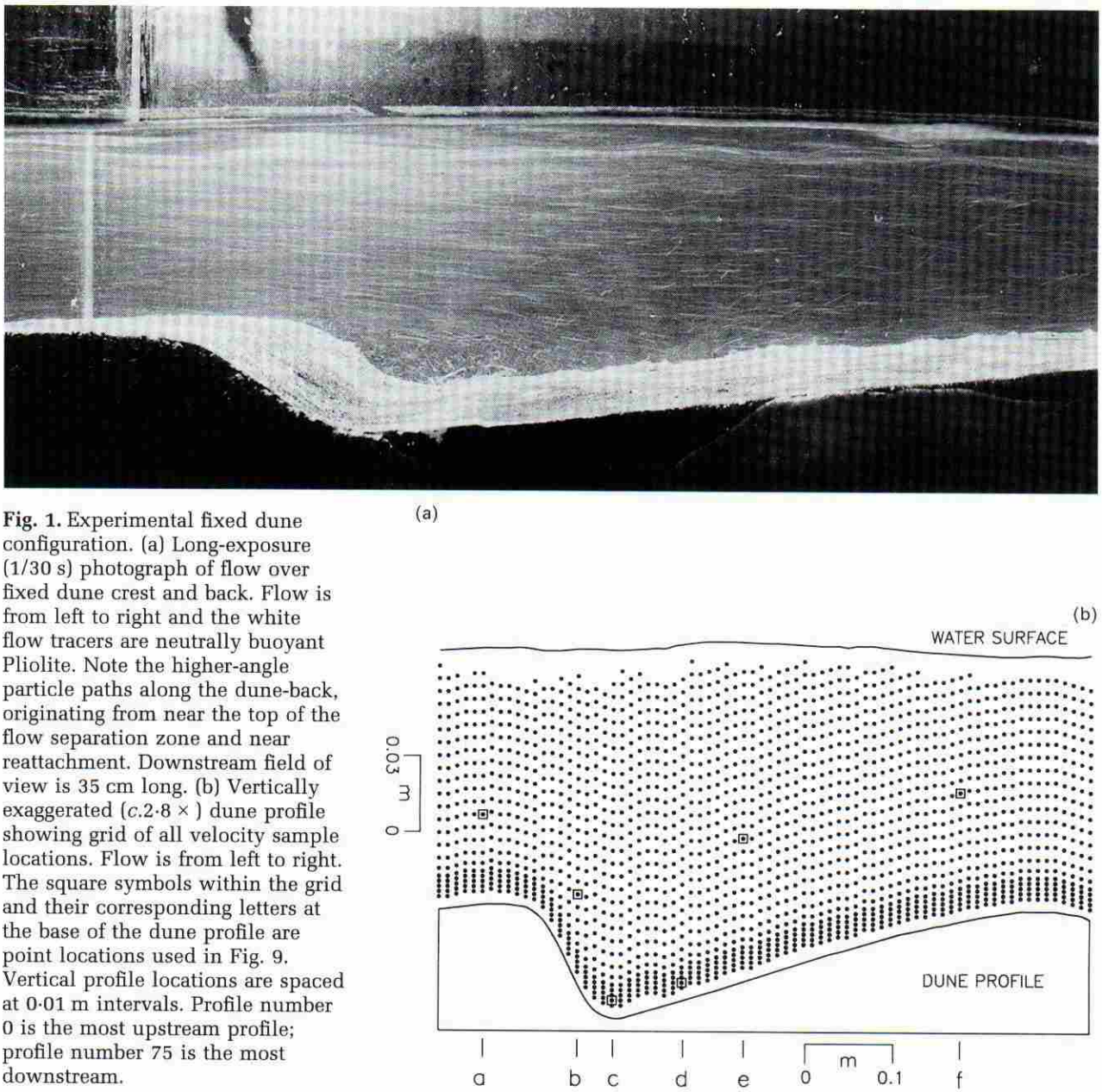

Fig. 1. Experimental fixed dune configuration. (a) Long-exposure (1/30 s) photograph of flow over fixed dune crest and back. Flow is from left to right and the white flow tracers are neutrally buoyant Pliolite. Note the higher-angle particle paths along the dune-back, originating from near the top of the flow separation zone and near reattachment. Downstream field of view is 35 cm long. (b) Vertically exaggerated (*c.*2·8 ×) dune profile showing grid of all velocity sample locations. Flow is from left to right. The square symbols within the grid and their corresponding letters at the base of the dune profile are point locations used in Fig. 9. Vertical profile locations are spaced at 0·01 m intervals. Profile number 0 is the most upstream profile; profile number 75 is the most downstream.

$$H=|uv|/u'v' \qquad (8)$$

where $u'v'$ is the product of the time-averaged RMS values at-a-point and $u=u_i-\bar{U}$ and $v=v_i-\bar{V}$. Using different threshold values allows discrimination of the contribution of high-magnitude events within each quadrant to the total turbulent signal. Typical threshold values associated with burst detection (quadrant-2 events) range from 1·07 (Bogard & Tiederman, 1986) to 4·0 to 4·5 (Lu & Willmarth, 1973; Willmarth & Lu, 1974), whereas values of 2 to 3 have been used for quadrant-4 events (op. cit.). Because of the lack of data and reliable guidelines concerning event thresholds in non-canonical boundary layers (*sensu* Robinson, 1991), no attempt was made to constrain the time between successive measurements, thus enabling differentiation between single-event and multiple-event ejections (see Luchik & Tiederman, 1987).

Flow visualization over the dunes was accomplished using long-exposure 35 mm photographs of neutrally buoyant Pliolite tracer particles (see Bridge & Best, 1988; Fig. 1a). These photographs provided visual evidence of the local streamlines and instantaneous turbulent events over the dune profile.

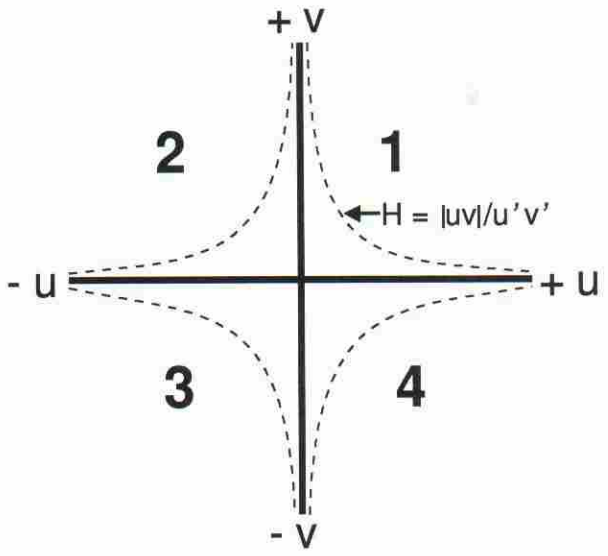

Fig. 2. Quadrants of the instantaneous *uv* plane. The threshold value, *H*, is determined through comparison of the instantaneous *uv* product with the product of the *u* and *v* RMS values. Quadrants 2 and 4 denote 'ejections' and 'sweeps' of turbulent boundary layer studies, whereas quadrants 1 and 3 depict outward and inward interactions.

RESULTS

Mean flow field

Vertical profiles of the mean values of the downstream and vertical velocity components at selected locations (Figs 3 and 4) and contour maps of the full flow field (Fig 5a,b) illustrate the characteristic features of flow over the fixed dunes. The greatest downstream velocities occur just prior to and at the dune crest (Figs 3a and 5a) and are followed by a sudden expansion and separation of flow just downstream of the crest. Negative horizontal flow velocities in the separation zone may reach $-0{\cdot}1$ to $-0{\cdot}2\,\bar{U}$, with profiles showing intense shear (drag) across the separation cell (Fig. 3c). The mean distance from the separation point to flow reattachment, X_r, is $4{\cdot}25\,h$ (where h is the bedform height), in good agreement with previous studies (Engel, 1981; Nelson & Smith, 1989a). Downstream of reattachment, three distinct layers can be observed (Fig. 3d): (1) the newly formed internal boundary layer ($\leq 0{\cdot}1\,Y$); (2) the advecting and diffusing mixing zone along the shear layer (the wake; $\geq 0{\cdot}1\,Y$ to $\leq 0{\cdot}5\,Y$); and (3) the still unaffected outer region of the flow ($\geq 0{\cdot}5\,Y$). These profiles illustrate the dominant effect of flow separation on the local flow field. By the next crest, the wake region has diffused and mixed completely, the internal boundary layer has developed fully and merged with the outer flow region, and nearly uniform flow conditions prevail, which are identical to those of the previous crest (see Figs 3f and 5a).

The time-averaged vertical velocity over the dune crest is close to zero (Figs 4a and 5b). As flow expansion and separation begin, streamlines are directed towards the bed and very large negative velocities ($-0{\cdot}03$ to $-0{\cdot}06$ m s^{-1}) occur just downstream of the crest and downstream of the separation cell (Figs 4b,c and 5b). Positive vertical velocities within the separation cell demonstrate the strong circulation pattern, especially near the dune slip-face, where velocities approach $0{\cdot}06$ m s^{-1} (Fig. 5b). Topographic forcing causes flow acceleration over the next dune back, producing positive vertical velocities near the bed (Figs 4d,e and 5b; note that the laser is fixed in an orthogonal position relative to the flume slope throughout the experiments). By the next dune crest, flow is essentially identical to the previous crest (Figs 4a,f and 5b).

The general information provided by these mean velocity maps confirms previous studies of flow over dunes (see references above; Table 1) as well as investigations of flow over negative steps (e.g. Bradshaw & Wong, 1972; Etheridge & Kemp, 1978, 1979; Nakagawa & Nezu, 1987; Adams & Eaton, 1988). However, these maps provide the most comprehensive results detailing the entire flow field and serve to demonstrate the quasi-equilibrium flow over dunes, as shown by the symmetry of velocity over adjacent dune crests. Because the mean flow fields are both well-defined and well-constrained, the turbulence structure and velocity time-series may be investigated with confidence.

Velocity moments and Reynolds stresses

Contour maps of the RMS of the downstream (u') and vertical (v') velocities are shown in Fig. 5c,d. Maximum u' values, up to $0{\cdot}32$ m s^{-1}, occur at and just downstream of reattachment (Figs 5c and 3d) with local high values (from $0{\cdot}12$ to $0{\cdot}24$ m s^{-1}) located within and just downstream of the separation cell. At a distance approximately $0{\cdot}6\,\lambda$ downstream from the crest (where λ is dune wavelength), u' values have reduced to levels similar to those of the free-stream (Figs 5c, 3a and 3f).

Maximum v' values, up to $0{\cdot}09$ m s^{-1}, occur within and above the zone of flow separation along the shear layer (Figs 4c and 5d). The region

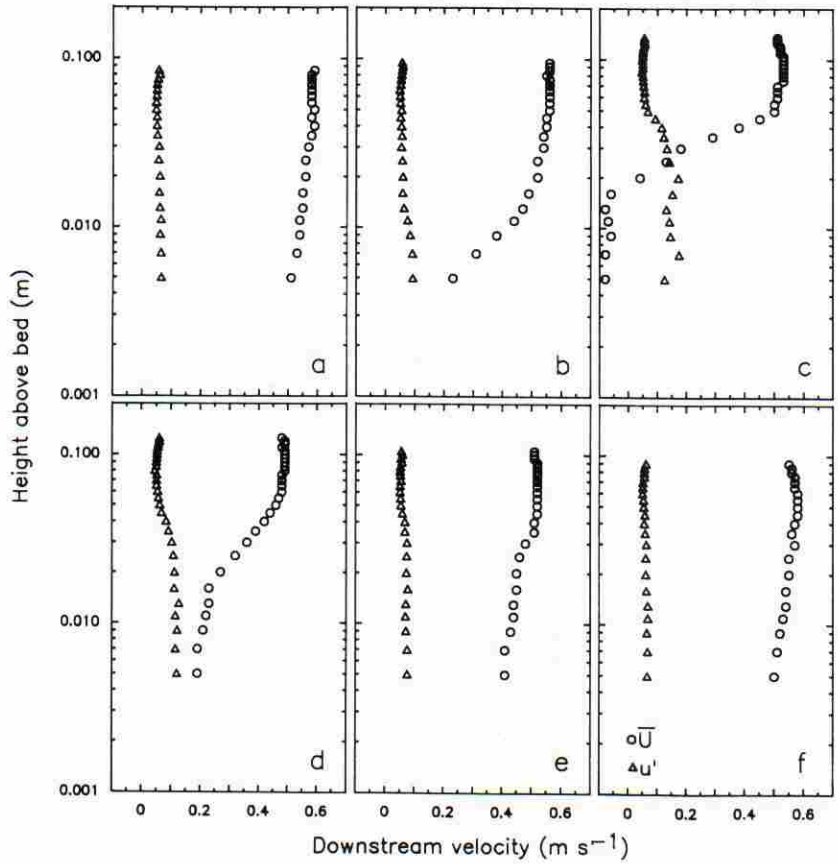

Fig. 3. Vertical profiles of $\bar{U}$ and u' over fixed dunes at selected locations (see Fig. 1b); (a) just upstream of dune crest (profile number 6); (b) just downstream of dune crestline (profile 13); (c) within the centre of flow separation (profile number 21); (d) just downstream of reattachment (profile number 31); (e) mid-back of dune (profile number 52); (f) just upstream of dune crest (profile number 68).

of high v' values (from 0·05 to 0·08 m s^{-1}) extends from the dune crestline towards the next crest, completely encapsulating the shear layer produced at separation. Because this region is detached from the bed and the mean velocity is removed from these determinations, these relatively high v' values are not the result of topographic forcing of the flow over the next dune back but are associated with eddy shedding along the shear layer. Low v' values (from 0·01 to 0·03 m s^{-1}) are present within the zone of flow separation along the dune slip-face and near the water surface.

The spatial variation of skewness for both the downstream and vertical velocity distributions is shown in Fig. 6a,b. A strong positive skewness in the downstream component is located within the zone of flow separation and especially near the crestline, representing the mixing of higher velocity fluid above the shear layer with the lower velocity fluid of the separation cell (Fig. 6a). A zone of slightly negative skewness values along the shear layer also can be observed, reflecting the ejection of lower than average velocity fluid along this region (see below).

The skewness of the vertical velocity component shows a marked region of positive values along the shear layer (Fig. 6b; see also Itakura & Kishi, 1980), diagnostic of fluid ejection along this layer into the outer flow. Small zones of positive skewness also occur just upstream of the crest, just downstream of reattachment and at the base of the separation cell. Relatively high negative vertical skewness values are restricted to the centre of the separation cell (Fig. 6b), reflecting entrainment of low-velocity fluid into this zone.

A contour map of the spatial variation in Reynolds stress (Fig. 6c) shows that maximum τ_r values (up to 9 Pa) occur both at and just downstream of reattachment and along the shear layer extending from the crestline to approximately 0·5 λ. As expected, the maximum exchange of fluid momentum occurs along the shear layer, where both high u' and v' values are observed. Zero and slightly negative τ_r values near the water surface reflect the very low shear in this region and the influence of the free-water surface. Nelson *et al.* (1993) observed similar zero and negative τ_r values and suggested that exact equilibrium flow over the fixed bedforms was not achieved.

These higher moment velocity and Reynolds stress determinations illustrate that fluid turbulence is greatest in the separation zone, at reattachment and along the shear layer produced

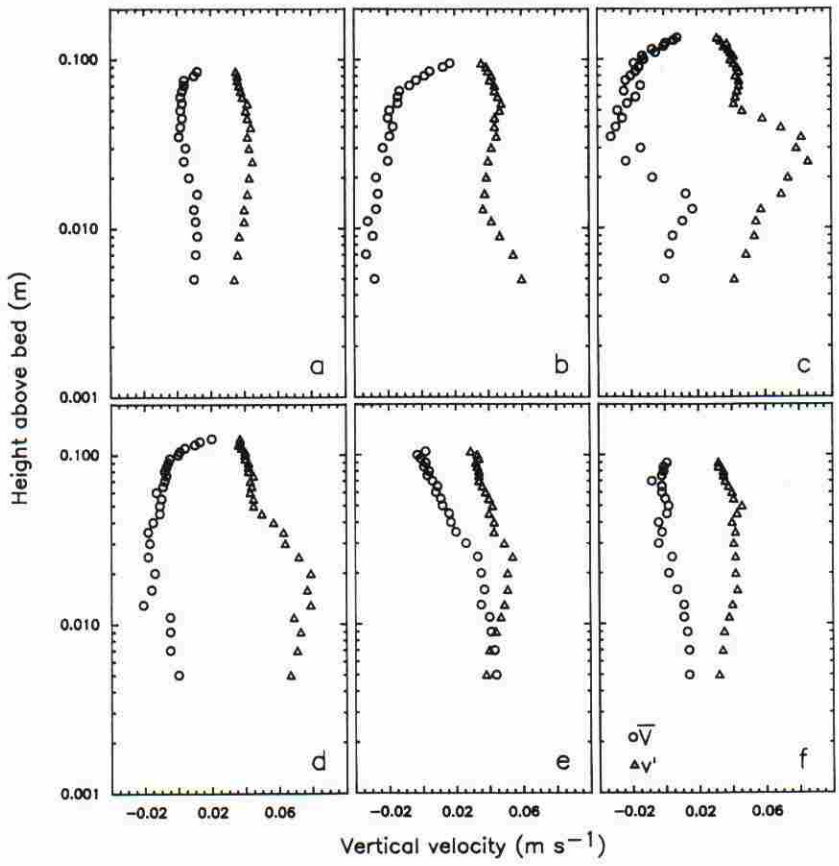

Fig. 4. Vertical profiles of $\overline{V}$ and v' over fixed dunes at selected locations (see Fig. 1b): (a) just upstream of dune crest (profile number 6); (b) just downstream of dune crestline (profile number 13); (c) within the centre of flow separation (profile number 21); (d) just downstream of reattachment (profile number 31); (e) mid-back of dune (profile number 52); (f) just upstream of dune crest (profile number 68).

through flow separation. Turbulence production associated with the dune flow field is dominated by Kelvin–Helmholtz instabilities associated with the shear layer (see also Müller & Gyr, 1982, 1986). Although previous studies have observed these high turbulence intensities (Müller & Gyr, 1982, 1986; Lyn, 1993; Nelson *et al.*, 1993; McLean *et al.*, 1994), none have quantified the magnitude of this turbulence nor have they delineated the morphology and downstream extent of this highly turbulent region.

Quadrant analysis

As described earlier, quadrant analysis examines the instantaneous uv product at-a-point in relation to some multiple (H; or hole size) of the time-averaged $u'v'$ value (Eq. 8). The representation of quadrant analysis most widely used is to determine the fractional contribution of those uv products greater than H to the time-averaged $-\overline{uv}$ (see Lu & Willmarth, 1973). For $H=0$, $-\overline{uv}_Q$, for each quadrant Q, is determined from

$$-\overline{uv}_Q = \frac{1}{n}\sum_{i=1}^{n} S(u_i - \bar{U})(v_i - \bar{V}) \qquad (9)$$

where the sorting factor, S, is equal to 1 if $u_i - \bar{U}$ $(=u)$ and $v_i - \bar{V}$ $(=v)$ fall into quadrant Q, otherwise $S=0$. For $H>0$, Eq. (9) is used, with $S=1$ if $|uv| \geq H$, otherwise $S=0$. Quadrants 2 and 4 provide an extraction of energy from the mean flow field to generate turbulence, hence producing the sign convention used in Eq. 7a (see Massey, 1989, p. 147). Negative contributions to the Reynolds stress in quadrants 1 and 3 denote motions that may be envisaged as extracting energy from turbulence to the mean flow (see discussions in Bradshaw, 1971; Landahl & Mollo-Christensen, 1986; Tritton, 1988). The results of quadrant analysis presented herein are: (1) the number of events in a given quadrant above a threshold value divided by the total number of observations for all quadrants (expressed as a percentage of the total); and (2) the number of events in a given quadrant above a threshold value divided by the total sample time (number of events per unit time; given in Hz). Note that the absolute data rate yielded by LDA is dependent on the optical configuration and hardware validation levels chosen for the LDA, although these were kept constant in this study. Because the absolute Reynolds stresses are zero or slightly negative near the free-water

surface, the results of using quadrant analysis in these regions have little physical significance.

Contour maps of the number and frequency of specific quadrant events, as a function of bed position and threshold value, are shown in Figs 6d, 7 and 8. The fractional contributions of each quadrant to $-\overline{uv}$ at different threshold values for six locations within the flow are shown in Fig. 9. The points in Fig. 9 (see Fig. 1b for their exact positions) were chosen to compare contributions from within the free-stream (Fig. 9a), the separation zone (Fig. 9c), near flow reattachment (Fig. 9d) and at three locations along the shear layer (Figs. 9b,e,f). At H=0, all quadrant contributions are similar to those documented in previous studies of both turbulent boundary layers over flat beds (e.g. Lu & Willmarth, 1973) and over bed topography in field investigations (e.g. Soulsby *et al.*, 1991; Clifford & French, 1993).

Quadrant-1 events over a threshold of 2 (Fig. 6d) show an increased occurrence within the separation zone and both at and downstream from reattachment. These regions probably are associated with the ejection away from the boundary of fluid that previously has been brought towards the bed within and along the separation-zone shear layer. Such motions are apparent from flow visualization near reattachment (Fig. 1a) and may provide one mechanism by which sediment is eroded from the trough area and lower dune back. However, these motions are restricted mainly to near the bed (Fig. 6d) and show a rapid dissipation vertically. Additionally, few zones of higher quadrant-1 occurrence exist downstream from $0{\cdot}6 \sim \lambda$, where the stoss slope flattens off towards the crestal shoulder. Quadrant-1 events exhibit similar contributions to $-\overline{uv}$ at all points, with only minor contributions over threshold values of 2 (see Figs 9 and 6d). However, within the separation zone (Fig. 9c), the absolute magnitude of quadrant-1 events is higher, with contributions up to a threshold of 9, although these large events quickly diminish by reattachment (Fig. 9d). McLean *et al.* (1994) have suggested that large quadrant-1 events, although providing a negative contribution to the local Reynolds stress, may be important in sediment transport.

The number of quadrant-3 events over a threshold value of 2 are localized at flow reattachment, where low-velocity fluid, possibly entrained from within the separation zone, is brought towards the bed (Fig. 7c). The higher values above the dune crest reflect flow convergence in this region. The fractional contribution of quadrant-3 events to $-\overline{uv}$ is concentrated primarily below a threshold of 3, except for slightly higher values within the flow separation zone (Fig. 9d).

At threshold values of both 2 and 4, quadrant-2 events occur most frequently along the separation-zone shear layer and near reattachment (Figs. 7a,d and 8b,d). This zone of frequent quadrant-2 events extends and enlarges downstream, almost reaching the next dune crest and achieving a thickness close to 4 cm ($\sim h$) over the next dune back. The frequency of these events, varying between 2 and 3·5 Hz for H=2 and between 1·0 and 1·5 Hz for H=4, produces Strouhal numbers of between 0·17 and 0·83 (using Eq. (2) and $\bar{U}$ and $\bar{U}_c$ from Table 2). These Strouhal numbers are similar to the value of 0·14 observed for eddy shedding behind dunes by Itakura & Kishi (1980), and for flow over hemispheres (0·1 to 0·4, Acarlar & Smith, 1987) and gravel clasts in natural rivers (0·12 and 6·60, Clifford *et al.*, 1993). The range in frequencies

Fig. 5. Contour maps of mean flow and turbulence parameters. Flow is from left to right, scale colour bar is given for each map and vertical exaggeration is *c.* 1·3 × . (a) time-averaged downstream velocity ($\bar{U}$); (b) time-averaged vertical velocity ($\bar{V}$); (c) downstream RMS velocity (u'); (d) vertical RMS velocity (v').

Fig. 6. Contour maps of flow and turbulence parameters. Flow is from left to right, scale colour bar is given for each map and vertical exaggeration is *c.* 1·3 × : (a) skewness of the downsteam velocity distribution (U_{skew}); (b) skewness of the vertical velocity distribution (V_{skew}); (c) turbulent Reynolds stress (τ_r); (d) normalized number (%) of quadrant-1 events occurring for H=2.

Fig. 7. Contour maps of flow and turbulence parameters. Flow is from left to right, scale colour bar is given for each map and vertical exaggeration is *c.* 1·3 × : (a) normalized number (%) of quadrant-2 events occurring for H=2; (b) normalized number (%) of quadrant-3 events occurring for H=2; (c) normalized number (%) of quadrant-4 events occurring for H=2; (d) frequency (Hz) of quadrant-2 events occurring for H=2.

Fig. 8. Contour maps of flow and turbulence parameters. Flow is from left to right, scale colour bar is given for each map and vertical exaggeration is *c.* 1·3 × : (a) frequency (Hz) of quadrant-4 events occurring for H=2; (b) normalized number (%) of quadrant-2 events occurring for H=4; (c) frequency (Hz) of quadrant-2 events occurring for H=4; (d) normalized number (%) of quadrant-4 events occurring for H=4.

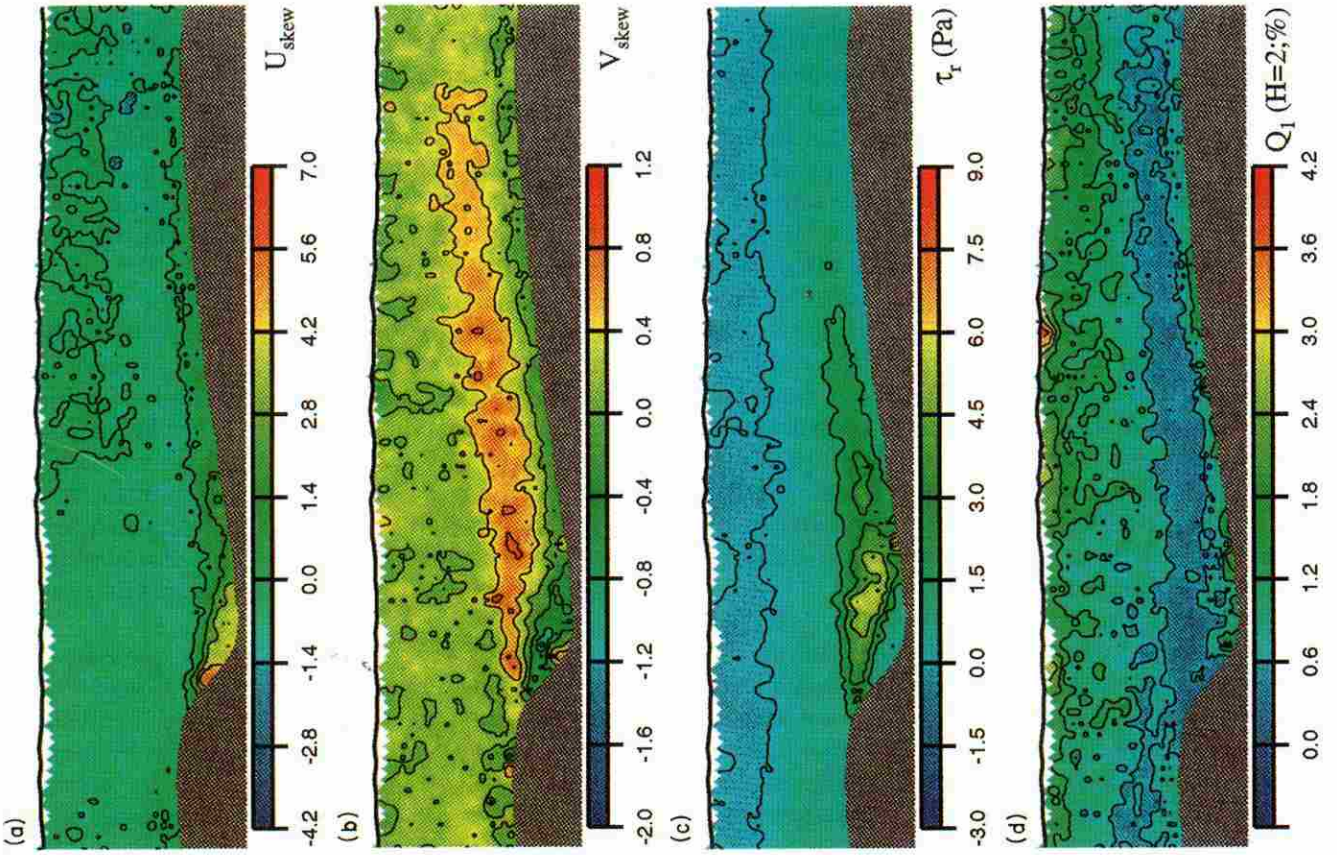
(a)
U (m s-1)
-0.2 -0.1 0.0 0.1 0.2 0.3 0.4 0.5 0.6
(b)
V (m s-1)
-0.060 -0.045 -0.030 -0.015 0.000 0.015 0.030 0.045 0.060
(c)
u′(m s-1)
0.00 0.04 0.08 0.12 0.16 0.20 0.24 0.28 0.32
(d)
v′(m s-1)
0.01 0.02 0.03 0.04 0.05 0.06 0.07 0.08 0.09

Fig. 5.

(a)
Uskew
-4.2 -2.8 -1.4 0.0 1.4 2.8 4.2 5.6 7.0
(b)
Vskew
-2.0 -1.6 -1.2 -0.8 -0.4 0.0 0.4 0.8 1.2
(c)
τr (Pa)
-3.0 -1.5 0.0 1.5 3.0 4.5 6.0 7.5 9.0
(d)
Q1 (H=2;%)
0.0 0.6 1.2 1.8 2.4 3.0 3.6 4.2

Fig. 6.

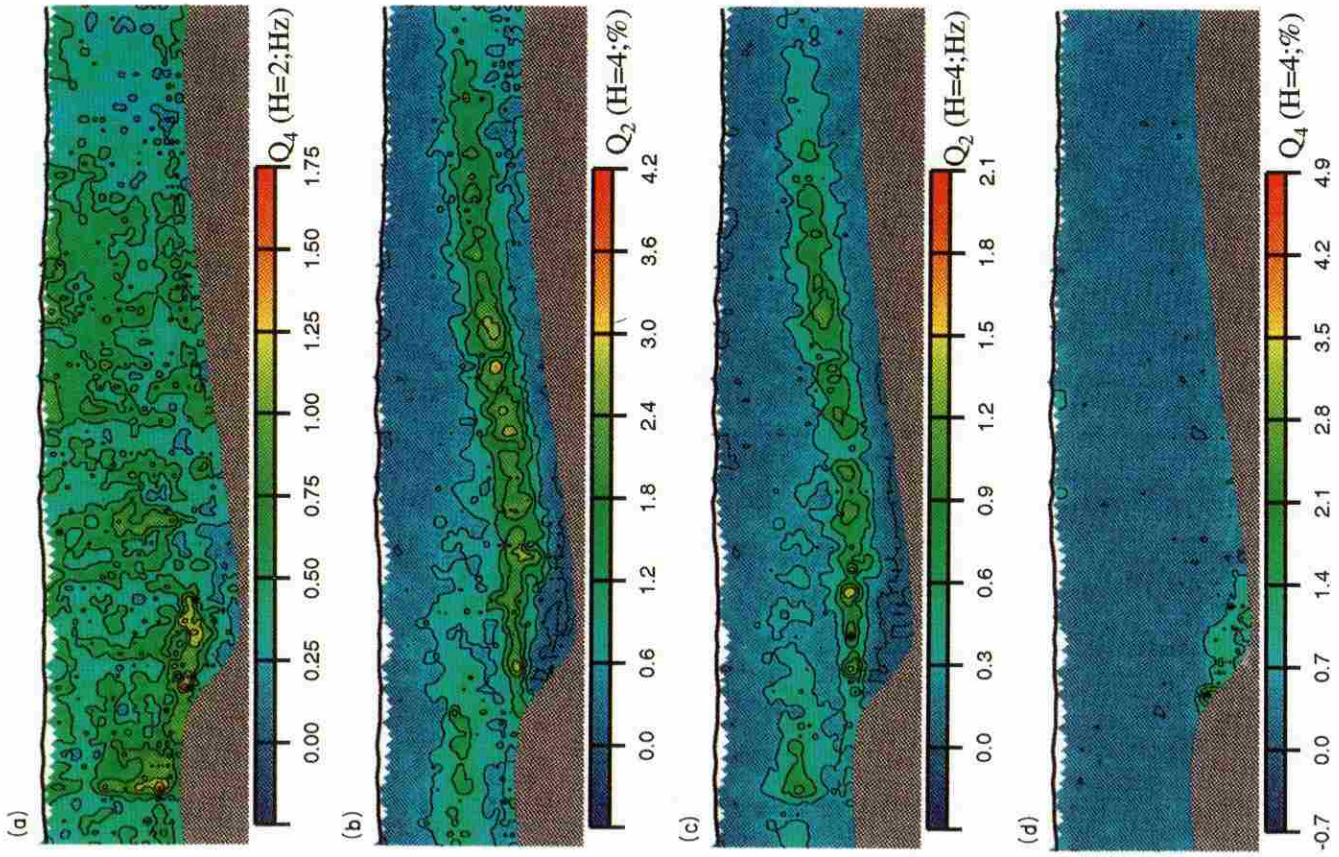
(a)
Q_2 (H=2;%)
0.0 1.2 2.4 3.6 4.8 6.0 7.2 8.4
(b)
Q_3 (H=2;%)
0.0 0.6 1.2 1.8 2.4 3.0 3.6 4.2
(c)
Q_4 (H=2;%)
0.0 1.2 2.4 3.6 4.8 6.0 7.2 8.4
(d)
Q_2 (H=2;Hz)
0.0 0.7 1.4 2.1 2.8 3.5 4.2 4.9

Fig. 7.

(a)
Q_4 (H=2;Hz)
0.00 0.25 0.50 0.75 1.00 1.25 1.50 1.75
(b)
Q_2 (H=4;%)
0.0 0.6 1.2 1.8 2.4 3.0 3.6 4.2
(c)
Q_2 (H=4;Hz)
0.0 0.3 0.6 0.9 1.2 1.5 1.8 2.1
(d)
Q_4 (H=4;%)
-0.7 0.0 0.7 1.4 2.1 2.8 3.5 4.2 4.9

Fig. 8.

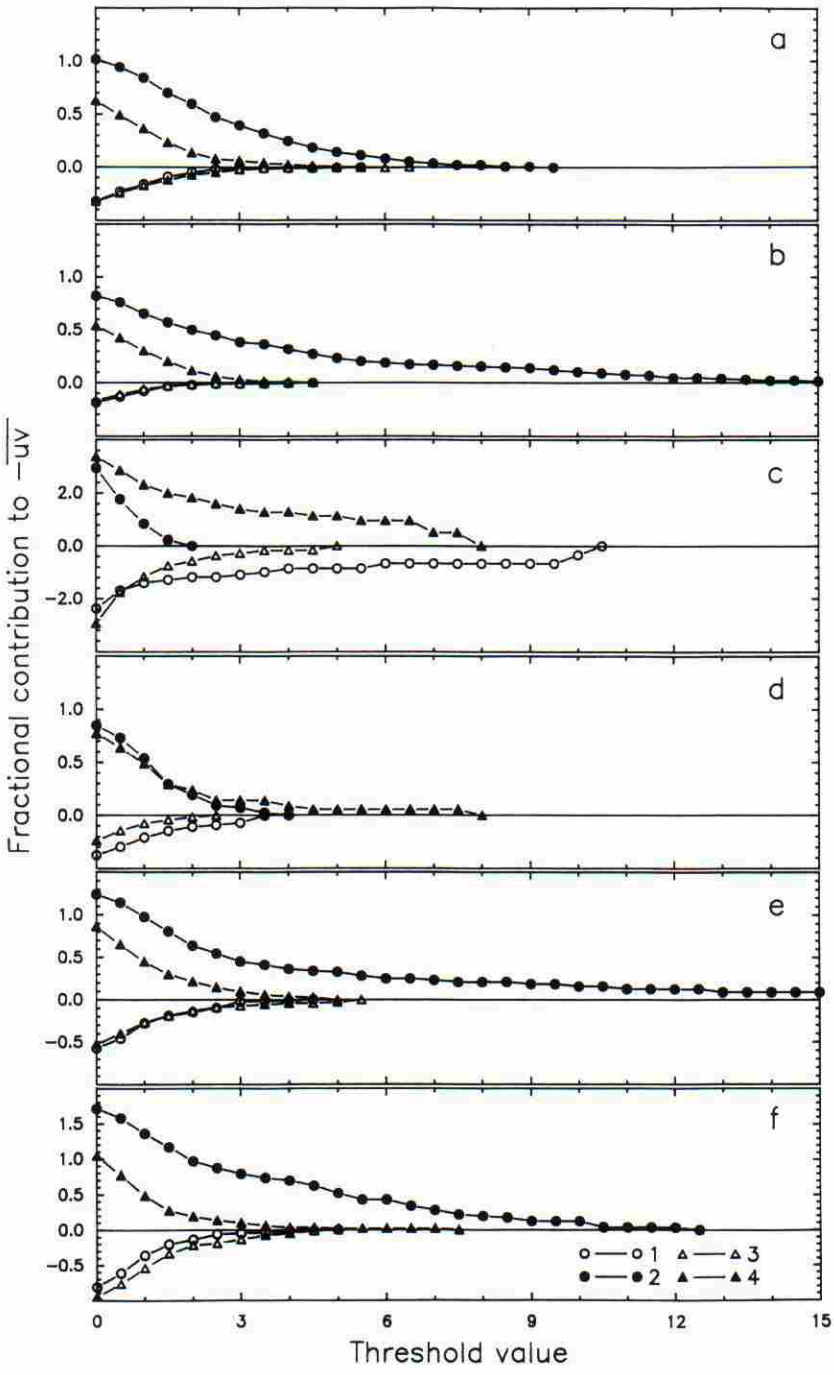

Fig. 9. Fractional contribution of each quadrant to $-\overline{uv}$ for varying values of *H*. Figure 1b shows the exact point locations at profiles 5, 16, 20, 28, 35 and 60.

measured here reflects both the intermittent shedding of eddies of different sizes and periods as well as vortex amalgamation and pairing along the shear layer (e.g. Müller & Gyr, 1986).

These results detailing the occurrence of high-magnitude quadrant-2 events illustrate that the source of dune-related 'bursting' or ejections reported previously (Jackson, 1976; Yalin, 1977, 1992; Lapointe, 1992) lies not in classical boundary layer bursting but in Kelvin–Helmholtz instabilities shed off the separation-zone shear layer. These data are supported by earlier experimental (Müller & Gyr, 1982, 1986; Levi, 1991) and field investigations (Rood & Hickin, 1989; Kostaschuk & Church, 1993), which document the occurrence of large eddies downstream from dune crests associated with high concentrations of suspended sediment. The occurrence of significant quadrant-2 events near reattachment also lends support to the field evidence of Kostaschuk &

Church (1993), who observed increased suspended sediment concentrations near the lower dune back as well as near the dune crest.

In general, quadrant-2 events dominate the fractional contribution to the local Reynolds stress irrespective of threshold value (Fig. 9). The contributions along the evolving shear layer initially increase (Fig. 9b,c), but as the shear layer zone mixes and dissipates downstream, these contributions decrease (Fig. 9f). It is apparent that relatively rare, high-magnitude ejection events (H>6) may be influential in Reynolds stress production and in the suspension of sediment (e.g. Sutherland, 1967; Grass, 1974; Sumer & Ogüz, 1978; Sumer & Deigaard, 1981). Not only are these high-magnitude events capable of transporting more and coarser grained sediment, but their frequency also will differ from that predicted using Eq. (2). The frequency of quadrant-2 events at threshold values of 6, 9 and 12 for the point analysed from profile 35 in Fig. 9e are 0·13, 0·08 and 0·05 Hz respectively. The presence of these larger magnitude, lower frequency events may explain some of the longer period events observed by Lapointe (1992) and Kostaschuk & Church (1993). Possible origins of these rarer and more energetic quadrant-2 events include: (1) temporal variations in the velocity gradients across the shear layer; (2) vortex interaction and pairing; and (3) lower frequency 'flapping' of the shear layer. Such longer period movement or 'flapping' of the entire shear layer has a dimensionless frequency, f_s, <0·1 (where $f_s=fX_r/\bar{U}$; see Simpson, 1989; Nelson *et al.*, 1993), giving estimated frequencies herein of approximately 0·3 Hz. The short sample lengths, however, prohibit further examination of this proposal. Furthermore, it is likely that the mixing layer is associated with streamwise vortices generated along the braids between the Kelvin–Helmholtz instabilities (see, for example, Metcalfe *et al.*, 1987; Lasheras & Choi, 1988; Silveira Neto *et al.*, 1993), which will also contribute to the ejection of fluid into the outer flow. Recent work on the interaction of outer region eddies with the near-wall structure (Myose & Blackwelder, 1994) also suggests that the sign of spanwise vortices may influence significantly the bursting process. Flow-transverse eddies impinging on a wall may either enhance or delay bursting depending on whether the spanwise vorticity is negative or positive (anticlockwise or clockwise respectively, when viewed in the streamwise, xy, plane). Such outer zone interaction and its influence on the ejection of fluid into the outer flow also may occur in the flow field behind bedforms and negative steps. Work has indicated that concave wall curvature also can modify significantly the turbulent boundary layer structure (Barlow & Johnston, 1988a,b), thus introducing additional complexities to flow over dunes, especially in the trough region and lower dune back.

Quadrant-4 events are most common bounding the separation zone and near reattachment (Figs 7c, 8a and 8d) and dominate the fractional contribution to the local Reynolds stress in these regions (Fig. 9c,d), reflecting the inrush of higher velocity fluid brought towards the bed along the shear layer. For H=4, the frequency of quadrant-4 events (Fig. 8d) is approximately 1·25 Hz along the upper part of the shear layer and above the dune crest. The remainder of the quadrant-4 field is characterized by frequencies of 0·25 to 0·75 Hz with no discernible pattern. Quadrant-4 events have been linked to the entrainment and bedload transport of sediment (e.g. Thorne *et al.*, 1989; Williams *et al.*, 1989; Williams, 1990) and the inrushes of fluid documented here may provide the high instantaneous shear stresses necessary for entrainment to occur both at reattachment and along the lower dune back (see Fig. 6c). This zone of frequency quadrant-4 events diffuses at *c.* 0·5λ, providing the potential for sediment eroded along the lower dune back to be deposited higher on the dune stoss side.

Bed shear stress

Following Smith & McLean (1977; Nelson & Smith, 1989b), the total spatially averaged boundary shear stress (τ_B) can be written as the sum of the skin-friction (τ_{SF}) and form-drag (τ_{FD}) components:

$$\tau_B=\tau_{SF}+\tau_{FD} \quad (10)$$

The total boundary shear stress, τ_B, was determined from measurements of the spatial average of the direct stress measurements well above the bedform (see Lyn, 1993; Nelson *et al.*, 1993). This was accomplished by averaging the values of τ_R from reattachment to the dune crest along constant height about the mean bed elevation. Because the measurements were staggered in space, each τ_R was sorted into 5-m bins, averaged and the mid-point of each bin plotted (Fig. 10). A region of linear stress exists between 0·035 and 0·070 m above the mean bed elevation. Linear regression through these points projected down to the zero mean bed height, corresponding to a hypothetical equivalent flat-bed flow, gives τ_B=1·68 Pa (Table 2).

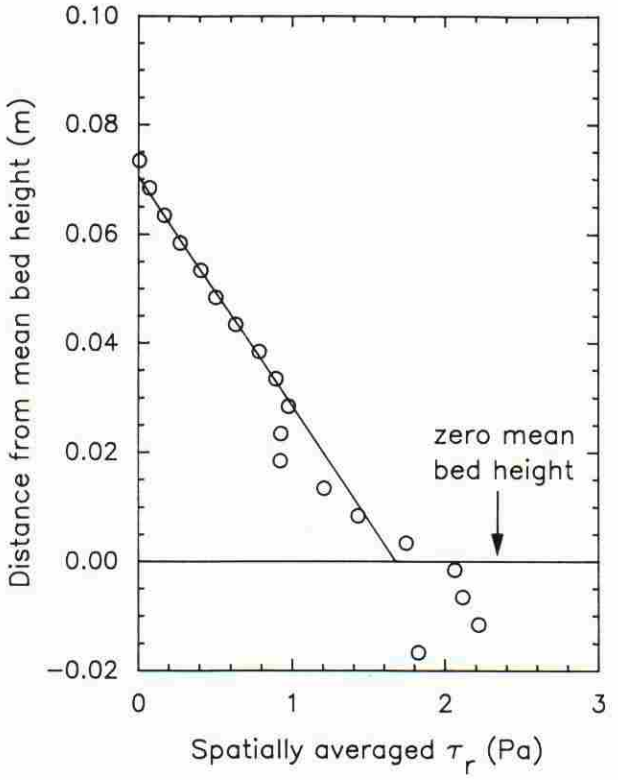

Fig. 10. Vertical variation of the spatially averaged Reynolds stress, τ_r, from reattachment to the dune crest about the mean bed elevation. A regression through the linear segment of the stress profile projected to the zero mean bed height is used to determine τ_B.

Skin-friction shear stress values could not be determined accurately from the near-bed velocities because an insufficient number of measurements were obtained within the internal boundary layer (see discussion in Nelson & Smith, 1988b). The average internal boundary layer thickness, y_*, was determined to be approximately 6·6 mm using

$$\frac{y_*}{y_0}=0{\cdot}1\left[\frac{\lambda}{y_0}\right]^{0{\cdot}8} \tag{11}$$

where the zero-velocity roughness height, y_0, is 0·008 mm (with $y_0=k_s/30{\cdot}2$; $k_s\sim D_{84}\sim 0{\cdot}25$ mm; Smith & McLean, 1977; Nelson *et al.*, 1993). By assuming that the velocity varies logarithmically between the lowest measured velocity (y=5 mm) and the bed, the skin-friction shear stress can be determined using 'the law of the wall'

$$\frac{U}{U_{*SF}}=\frac{1}{\kappa}\ln\left[\frac{\lambda}{y_0}\right] \tag{12a}$$

$$\tau_{SF}=\rho U_{*SF}^2 \tag{12b}$$

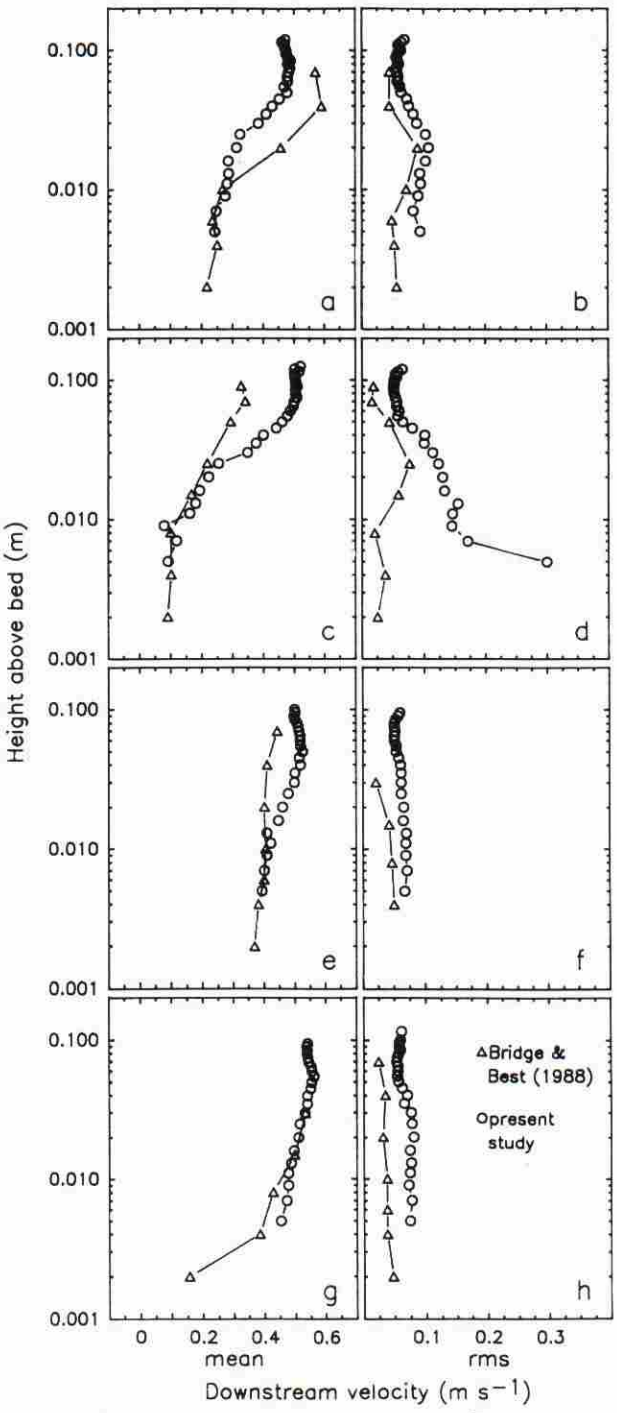

Fig. 11. Comparison of vertical profiles of $\bar{U}$ and u' over fixed dunes (circle symbols) to the mobile dunes (triangle symbols) of Bridge & Best (1988) at various locations (see Fig. 1b). (a) dune trough/lower dune back (using profile 35); (b) dune trough/lower dune back (using profile 27); (c) upper dune back (using profile 60); (d) upper dune back (using profile 50).

where U is the velocity measured at height y and von Karman's constant, κ, is 0·4. Values of τ_{SF} varied from near zero at reattachment to a

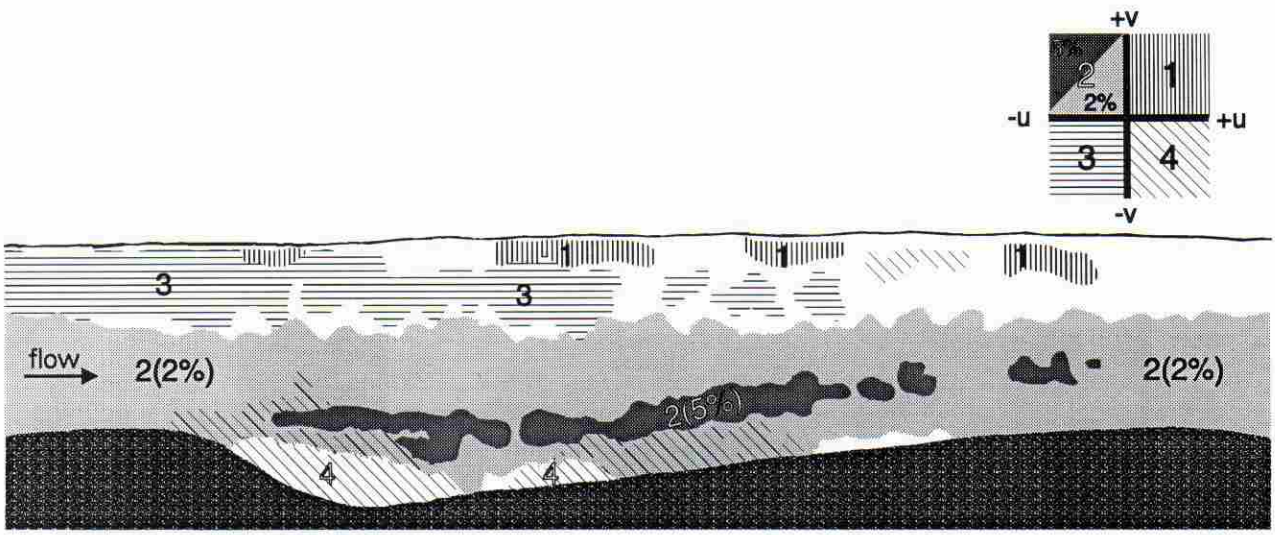

Fig. 12. Summary diagram of the spatial distribution of the percentage number of each quadrant event using $H=2$. For quadrant-2 events, both the 2% and the 5% contours are shown.

maximum of 1·08 Pa just upstream of the dune crest, with a spatial average of 0·61 Pa (Table 2). Using these τ_B and τ_{SF} values, bedform drag coefficients (C_D) of 0·20 and 0·16 were calculated using Eqs (13) and (14) in Nelson *et al.* (1993, p. 3942), respectively. These bedform drag coefficients are in close agreement with previous determinations (0·23, Smith & McLean, 1977; see Wiberg & Nelson, 1992; 0·23 to 0·45 and 0·18 to 0·31, Nelson *et al.*, 1993, using the same equations).

Comparison with mobile bed conditions

The bedform morphology and mean flow conditions used here compare well with the work of Bridge & Best (1988) upon which the present study was based (Table 2). Additional comparisons between the downstream velocity and RMS values for several positions over the troughs and backs of the dunes (Fig. 11) further demonstrate the similarity between mobile and fixed bed experiments. Mean velocities over the fixed dunes as a function of bed height are similar to the mobile dunes studied by Bridge & Best both in magnitude (Fig. 11e,g) and in shape (Fig. 11a,c,g). Lower velocities observed near the bed (i.e. greater drag, larger roughness heights) in the mobile bed conditions are due to: (1) increased drag associated with the moving bed layer (e.g. Wiberg & Rubin, 1989; Bridge & Bennett, 1992; and references therein); and (2) decreased drag over immobile beds due to the much lower porosity of the concrete bedforms as compared with the mobile sand bed (e.g. Zippe & Graf, 1983; Mendoza & Zhou, 1992).

Although the shape of the vertical u' profiles for both mobile and immobile bed conditions are similar (Fig. 11b,d,f,h), the LDA measurements of u' are larger in magnitude, especially in detecting the high turbulence values associated with the shear layer (Fig. 11d). This difference is due to: (1) the poor resolution of the constant temperature anemometer (CTA) used by Bridge & Best (1988) as compared with the LDA; and (2) the inability of the CTA to detect negative velocities (flow reversals) within the separation zone. Furthermore, the velocity and turbulence measurements obtained by Bridge & Best inevitably were prone to varying dune morphology during collection periods. However, the results presented herein may be viewed as typical of flow conditions over equilibrium dunes generated in 0·3 mm diameter sand.

DISCUSSION

These data on flow and turbulence structure over fixed dunes have important implications for both the mechanisms of sediment transport, in relation to dune formation and stability, and the fluid dynamic distinction between ripples and dunes. A summary diagram of the location of high-magnitude turbulent events (for $H=2$) with respect to bed position is shown in Fig. 12. Frequent, high-magnitude quadrant-2 events (ejections) dominate the lower two-thirds of flow, both along the shear layer, where they arise due to

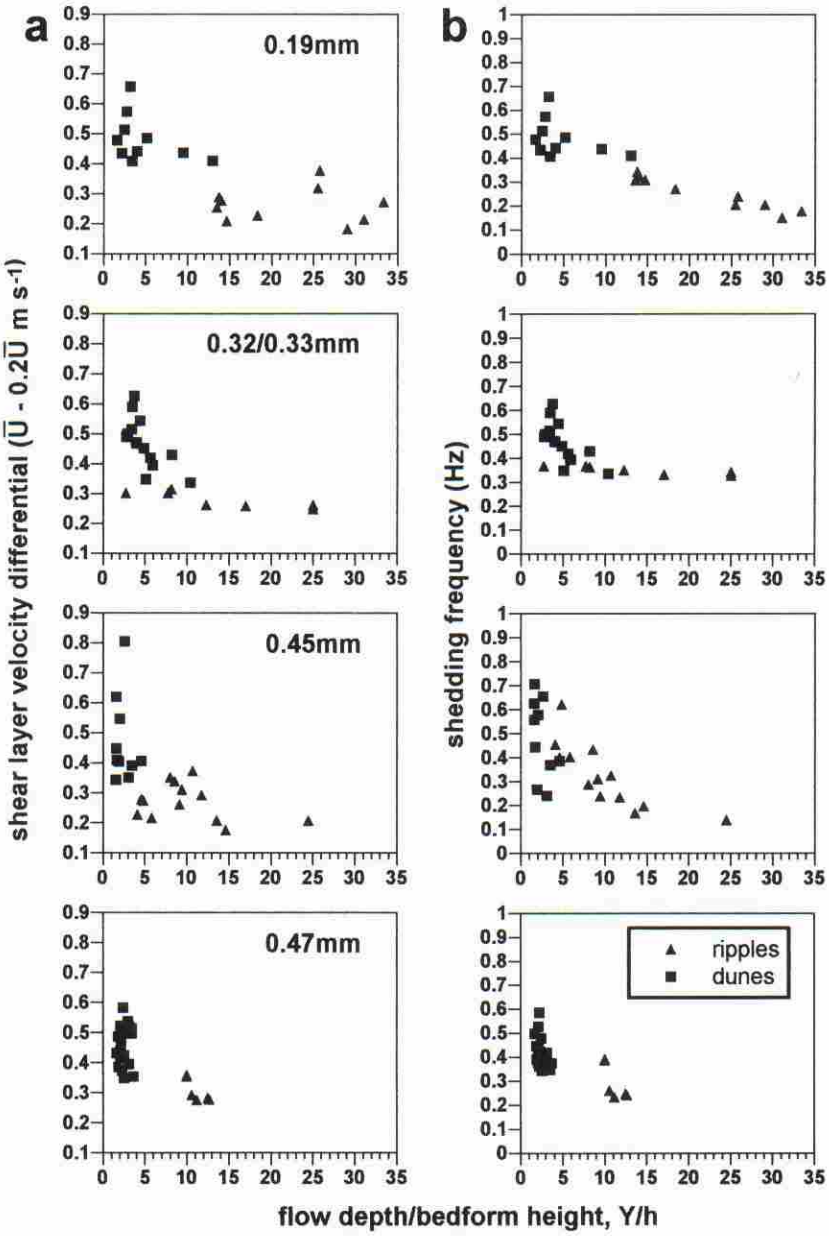

Fig. 13. Characteristics of the separation-zone shear layer across the ripple–dune transition for a variety of grain sizes (data from Simons *et al.*, 1961; Guy *et al.*, 1966). (a) the velocity differential across the free-shear layer ($\sim \bar{U} - 0{\cdot}2\ \bar{U}$) as a function of the ratio of flow depth to bedform height (Y/h), and, (b) eddy shedding frequency determined using Eq. (2) across the ripple–dune transition.

Kelvin–Helmholtz instabilities, and near the reattachment region. As discussed by Bennett & Best (1995), these quadrant-2 events provide a mechanism for the entrainment and suspension of sediment. This contention is supported in two ways: (1) the observation of high suspended sediment concentrations associated with 'boils' (Matthes, 1947; Coleman, 1969; Jackson, 1976; Rood & Hickin, 1989; Kostaschuk & Church, 1993) and similar velocity signals (Lapointe, 1992); and (2) the high positive skewness values of the vertical velocity distributions along the shear layer, which produce an anisotropy in vertical turbulence (see also Itakura & Kishi, 1980). Such anisotropy has been invoked as a mechanism for the maintenance of a suspended load (Bagnold, 1966; Leeder, 1983; Wei & Willmarth, 1991).

Frequent, high-magnitude quadrant-4 events dominate flow within the separation zone, at reattachment and at the dune crest (Fig. 12), demonstrating the movement of fluid towards the boundary along the shear layer, the impact of vortices on the bed and flow convergence over the crest. These turbulent events are capable of entraining sediment (e.g. Thorne *et al.*, 1989; Williams *et al.*, 1989; Williams, 1990) and provide evidence for the erosion and transport of sediment over the lower stoss of the dune and deposition high on the dune crest. Quadrant-1 events (Fig. 6d) may also play a role in sediment

entrainment in the reattachment region and add to the downstream sediment flux (see also McLean *et al.*, 1994).

This spatial pattern of entrainment, transport, suspension and deposition of sediment is controlled by the formation and downstream extent of the separation-zone shear layer (see Figs 5–8). The magnitude and frequency of ejection events will be determined by the velocity gradient across the shear layer and hence the rotational velocity of the Kelvin–Helmholtz instabilities that are generated. If we assume that mean velocity within the separation zone near the shear layer is approximately 0·2 $\bar{U}$ (see, for example, Etheridge & Kemp, 1978; Nakagawa & Nezu, 1987), then the velocity differential across the shear layer ($\sim \bar{U} - 0{\cdot}2\ \bar{U}$) can be estimated from data obtained across the ripple–dune transition in a range of sediment sizes (Fig. 13). These plots illustrate that, for any one grain size, once $Y/h \leq \sim 5$, the velocity differential across the shear layer increases rapidly and dunes become the stable bedform. The velocity differential across the shear layer may be viewed as being proportional to the turbulence intensity both within the shear layer and near the reattachment region. Previous work on negative steps has also demonstrated that the shear layer exerts a significantly greater influence on the entire flow field when the step height becomes a substantial fraction of the flow depth (Bradshaw & Wong, 1972). Additionally, dunes may exhibit a higher frequency of eddy shedding as compared with ripples (using Eq. (2); Fig. 13b). Hence, once a bedform reaches a certain height within the flow (perhaps by amalgamation of two 'rogue' ripples, see Leeder, 1980), then the velocity differential across the shear layer increases and quadrant-2 and -4 events become larger and more frequent, increasing the downstream sediment flux. Considerations of this turbulence structure are absent in linear stability analysis, suggesting that other processes may be responsible for the formation and hydraulic stability of dunes (see also McLean & Smith, 1986; McLean, 1990; Nelson *et al.*, 1993). It should be noted that the mean velocity, bed shear stress and sediment transport rate also increase across the ripple–dune transition. The larger flow depth above rippled beds also allows for greater mixing and dissipation of the low-magnitude, low-frequency eddies associated with the separation-zone shear layer. Therefore, dunes appear to be differentiated from ripples by possessing larger magnitude, higher frequency eddies, which can translate through the entire flow depth before becoming fully mixed. This also correlates broadly with the downstream extent of the shear layer, whose vertical thickness is approximately equal to dune height and whose downstream extent is approximately equal to dune length.

CONCLUSIONS

Detailed measurements of the downstream and vertical components of velocity over fixed, two-dimensional bedforms in a laboratory channel have defined the typical turbulence structure associated with dunes. High turbulence intensities and positive vertical skewness values, the result of high-magnitude fluid ejections due to Kelvin–Helmholtz instabilities, dominate the free shear layer bounding the flow separation zone. Such instabilities are the source of dune-related macroturbulence. The spatial distribution of specific turbulent events also provides possible mechanisms for the entrainment, transport and suspension of sediment associated with dunes. The formation, growth and downstream extent of the separation-zone free shear layer and its associated instabilities may ultimately control the formation, hydraulic stability and differentiation of ripples and dune bedforms in unidirectional flows.

ACKNOWLEDGMENTS

We are grateful for grants from the Natural Environment Research Council (Grants GR3/8235 & GR9/564) and Universities Funding Council which have allowed this work to be undertaken. Mike Leeder and John Bridge offered many useful comments on this topic during the course of this research, and Neil Woodhouse provided valuable technical support. We thank Jürgen Fredsøe and Steve McLean for their constructive reviews. An ASCII file of the mean velocity and moments data from these experiments is available from the authors on provision of a 3·5″ disk.

REFERENCES

Acarlar, M.S. and Smith, C.R. (1987) A study of hairpin vortices in a laminar boundary layer. Part 1. Hairpin vortices generated by a hemisphere protuberance. *J. Fluid Mech.*, **175**, 1–41.

Adams, E.W. and Eaton, J.K. (1988) An LDA study of backward-facing step flow, including the effects of velocity bias. *J. Fluids Eng.*, **110**, 275–282.

Allen, J.R.L. (1982) *Sedimentary Structures: their Character and Physical Basis.* Elsevier, Amsterdam, 539 pp.

Allen, J.R.L. (1984) Parallel lamination developed from upper-stage plane beds: a model based on larger coherent structures of the turbulent boundary layer. *Sediment. Geol.*, **39**, 227–242.

Bagnold, R.A. (1966) An approach to the sediment transport problem from general physics. *U.S. geol. Surv. Prof. Pap.* **422-I**.

Barlow, R.S. and Johnston, J.P. (1988a) Structure of a turbulent boundary layer on a concave surface. *J. Fluid Mech.*, **191**, 137–176.

Barlow, R.S. and Johnson, J.P. (1988b) Local effects of large-scale eddies on bursting in a concave boundary layer. *J. Fluid Mech.*, **191**, 177–195.

Bennett, S.J. and Best, J.L. (1995) Structure of turbulence over two-dimenional dunes. In: *Sediment Transport Mechanisms in Coastal Environments and Rivers* (Ed. by M. M. Berlorgey and J. F. A. Sleath), in press.

Best, J.L. (1995) The fluid dynamics of small-scale alluvial bedforms. In: *Advances in Fluvial Dynamics and Stratigraphy* (Ed. by P.A. Carling and M. Dawson), in press.

Bogard, D.G. and Tiederman, W.G. (1986) Burst detection with single-point velocity measurements. *J. Fluid Mech.*, **162**, 389–413.

Bradshaw, P. (1971) *An Introduction to Turbulence and its Measurement.* Pergamon Press, Oxford, 218 pp.

Bradshaw, P. and Wong, F.Y.F. (1972) The reattachment and relaxation of a turbulent shear layer. *J. Fluid Mech.*, **52**, 113–135.

Bridge, J.S. and Bennett, S.J. (1992) A model for the entrainment and transport of sediment grains of mixed sizes, shapes and densities. *Water Resour. Res.*, **28**, 337–363.

Bridge, J.S. and Best, J.L. (1988) Flow, sediment transport and bedform dynamics over the transition from dunes to upper-stage plane beds: implications for the formation of planar lamination. *Sedimentology*, **35**, 753–763.

Buchhave, P., George, W.K., Jr and Lumley, J.L. (1979) The measurement of turbulence with the laser-Doppler anemometer. *Ann. Rev. Fluid Mech.*, **11**, 443–503.

Clifford, N.J. and French, J.R. (1993) Monitoring and analysis of turbulence in geophysical boundaries: some analytical and conceptual issues. In: *Turbulence: Perspectives on Flow and Sediment Transport* (Ed. by N. J. Clifford, J. R. French and J. Hardisty), pp. 93–120. Wiley, Chichester.

Clifford, N.J., Hardisty, J., French, J.R. and Hart, S. (1993) Downstream variation in bed material characteristics: a turbulence-controlled form–process feedback mechanism. In: *Braided Rivers* (Ed. by J. L. Best and C. S. Bristow), *Spec. Publ. geol. Soc. London*, **74**, 89–104.

Coleman, J.M. (1969) Brahmaputra River: channel processes and sedimentation. *Sediment. Geol.*, **3**, 129–239.

Costello, W.R. (1974) *Development of bed configurations in coarse sands.* PhD thesis, Massachusetts Institute of Technology, Cambridge.

DANTEC (1991) *Particle Dynamics Analyzer: User's Manual.* 107 pp. Dantec Elektronik.

Dinehart, R.L. (1989) Dune migration in a steep, coarse-bedded stream. *Water Resour. Res.*, **25**, 911–923.

Dinehart, R.L. (1992) Evolution of coarse gravel bed forms: field measurements at flood stage. *Water Resour. Res.*, **28**, 2667–2689.

Durst, F., Melling, A. and Whitelaw, J.H. (1987) *Principles and Practice of Laser-Doppler Anemometry*, 2nd edn. G. Braun, Karlsruhe, 405 pp.

Engel, P. (1981) Length of flow separation over dunes. *ASCE J. Hydraul. Div.*, **107**, 1133–1143.

Engelund, F. and Fredsøe, J. (1982) Sediment ripples and dunes. *Ann. Rev. Fluid Mech.*, **14**, 13–37.

Etheridge, D.W. and Kemp, P.H. (1978) Measurements of turbulent flow downstream of a rearward-facing step. *J. Fluid Mech.*, **86**, 545–566.

Etheridge, D.W. and Kemp, P.H. (1979) Velocity measurements downstream of rearward-facing steps, with reference to bed instability. *J. Hydrual. Res.*, **17**, 107–119.

Fehlman, H.M. (1985) *Resistance components and velocity distributions of open channel flows over bed forms.* MS thesis, Colorado State University, Ft Collins.

Gabel, S.L. (1993) Geometry and kinematics of dunes during steady and unsteady flows in the Calamus River, Nebraska, USA. *Sedimentology*, **40**, 237–269.

Gould, R.D. and Loseke, K.W. (1993) A comparison of four velocity bias correction techniques in laser Doppler velocimetry. *J. Fluids Eng.*, **115**, 508–514.

Grass, A.J. (1974) Transport of fine sand on a flat bed: turbulence and suspension mechanics. In: *Transport, Erosion and Deposition of Sediment in Turbulent Streams, Proc. Euromech 48*, pp. 33–34. Tech. Univ. of Denmark.

Guy, H.P., Simons, D.B. and Richardson, E.V. (1966) Summary of alluvial channel data from flume experiments, 1956–1961. *U.S. geol. Surv. Prof. Pap.*, **462-I**, 96 pp.

Hayashi, T. (1970) Formation of dunes and antidunes in open channels. *ASCE J. Hydraul. Div.*, **96**, 357–366.

Hubbell, D.W., Stevens, H.H., Skinner, J.V. and Beverage, J.P. (1987) Laboratory data on coarse-sediment transport for bedload sampler calibrations. *U.S. geol. Surv., Water Supply Pap.* **W2299**, 31 pp.

Itakura, T. and Kishi, T. (1980) Open channel flow with suspended sediment on sand waves. In: *Proc. 3rd International Symposium on Stochastic Hydraulics* (Ed. by H. Kikkawa and Y. Iwasa), pp. 599–609. Int. Ass. of Hydraul. Res., Tokyo.

Jackson, R.G. (1976) Sedimentological and fluid-dynamic implications of the turbulent bursting phenonemon in geophysical flows. *J. Fluid Mech.*, **77**, 531–560.

Johns, B., Soulsby, R.L. and Chesher, T.J. (1990) The modelling of sandwave evolution resulting from suspended and bed load transport of sediment. *J. Hydraul. Res.*, **28**, 355–374.

Johns, B., Soulsby, R.L. and Xing, J. (1993) A comparison of numerical model experiments of free surface flow over topography with flume and field observations. *J. Hydraul. Res.*, **31**, 215–228.

Kennedy, J.F. (1963) The mechanics of dunes and antidunes in erodible-bed channels. *J. Fluid Mech.*, **16**, 512–544.

Kennedy, J.F. (1969) The formation of sediment ripples, dunes and antidunes. *Ann. Rev. Fluid Mech.*, **1**, 147–168.

Korchokha, Y.M. (1968) Investigation of the dune movement of sediments on the Polomet' River. *Sov. Hydrol.*, **11**, 541–559.

Kostaschuk, R.A. and Church, M.A. (1993) Macroturbulence generated by dunes: Fraser River, Canada. *Sediment. Geol.*, **85**, 25–37.

Landahl, M.T. and Mollo-Christensen, E. (1986) *Turbulence and Random Processes in Fluid Mechanics.* Cambridge University Press, Cambridge, 154 pp.

Lane, E.W. (1944) A new method of sediment transportation. *Trans. Am. Geophys. Union*, **25**, 900.

Lapointe, M.F. (1992) Burst-like sediment suspension events in a sand bed river. *Earth Surf. Process. Landforms*, **17**, 253–270.

Lasheras, J.C. and Choi, H. (1988) Three-dimensional instability of a plane free shear layer: an experimental study of the formation and evolution of streamwise vortices. *J. Fluid Mech.*, **189**, 53–86.

Leeder, M.R. (1980) On the stability of lower stage plane beds and the absence of ripples in coarse sands. *J. geol. Soc. London.*, **137**, 423–429.

Leeder, M.R. (1983) On the dynamics of sediment suspension by residual Reynolds stresses—confirmation of Bagnold's theory. *Sedimentology*, **30**, 485–491.

Levi, E. (1983) A universal Strouhal law. *J. Eng. Mech.*, **109**, 718–727.

Levi, E. (1991) Vortices in hydraulics. *J. Hydraul. Eng.*, **117**, 399–413.

Lu, S.S. and Willmarth, W.W. (1973) Measurements of the structure of the Reynolds stress in a turbulent boundary layer. *J. Fluid Mech.*, **60**, 481–511.

Luchik, T.S. and Tiederman, W.G. (1987) Timescale and structure of ejections and bursts in turbulent channel flows. *J. Fluid Mech.*, **174**, 529–552.

Lyn, D.A. (1993) Turbulence measurements in open-channel flows over artifical bed forms. *J. Hydraul. Eng.*, **119**, 306–326.

Massey, B.S. (1989) *Mechanics of Fluids*, 6th edn. Chapman & Hall, London.

Matthes, G.H. (1947) Macroturbulence in natural stream flow. *Trans. Am. Geophys. Union*, **28**, 255–262.

McCorquodale, J.A. and Giratalla, M.K. (1973) Flow over natural and artifical ripples. In: *Proc. 15th Congr. Int. Ass. Hydraul. Res.*, **1**, pp. A22-1–A22-6. Istanbul.

McLean, S.R. (1990) The stability of ripples and dunes. *Earth Sci. Rev.*, **29**, 131–144.

McLean, S.R. and Smith, J.D. (1986) A model for flow over two-dimensional bed forms. *J. Hydraul. Eng.*, **112**, 300–317.

McLean, S.R., Nelson, J.M. and Wolfe, S.R. (1994) Turbulence structure over two-dimensional bedforms: implications for sediment transport. *J. Geophys. Res.*, **99**, 12729–12747.

Mendoza, C. and Shen, H.W. (1990) Investigation of turbulent flow over dunes. *J. Hydraul. Eng.*, **116**, 459–477.

Mendoza, C. and Zhou, D. (1992) Effects of porous bed on turbulent stream flow above bed. *J. Hydraul. Eng.*, **118**, 1222–1240.

Metcalfe, R.W., Orszag, S.A., Brachet, M.E., Menon, S. and Riley, J.J. (1987) Secondary instability of a temporally growing mixing layer. *J. Fluid Mech.*, **184**, 207–243.

Müller, A. and Gyr, A. (1982) Visualization of the mixing layer behind dunes. In: *Mechanics of Sediment Transport* (Ed. by B. M. Sumer and A. Müller), pp. 41–45. A.A. Balkema, Rotterdam.

Müller, A. and Gyr, A. (1986) On the vortex formation in the mixing layer behind dunes. *J. Hydraul. Res.*, **24**, 359–375.

Myose, R.Y. and Blackwelder, R.F. (1994) On the role of the outer region in the turbulent-boundary-layer bursting process. *J. Fluid Mech.*, **259**, 345–373.

Nakagawa, H. & Nezu, I. (1987) Experimental investigation on turbulent structure of backward-facing step flow in an open channel. *J. Hydraul. Res.*, **25**, 67–88.

Nelson, J.M. & Smith, J.D. (1989a) Flow in meandering channels with natural topography. In: *River Meandering* (Ed. by S. Ikeda and G. Parker), pp. 69–102. Am. Geophys. Union, Washington, DC. Water Res. Monogr. 12.

Nelson, J.M. and Smith, J.D. (1989b) Mechanics of flow over ripples and dunes. *J. Geophys. Res.*, **94**, 8146–8162.

Nelson, J.M., McLean, S.R. and Wolfe, S.R. (1993) Mean flow and turbulence fields over two-dimensional bed forms. *Water Resour. Res.*, **29**, 3935–3953.

Nezu, I. and Nakagawa, H. (1993) *Turbulence in Open-channel Flows.* Int. Ass. Hydraul. Res. Monograph Series, A.A. Balkema, Rotterdam, 281 pp.

Nezu, I., Nakagawa, H., Tominaga, A. and Yoshikawa, M. (1980) Visual study of large-scale vortical motions in open-channel flows. In: *Ann. Conf. Jap. Soc. civ. Engrs.*, Kansai-Branch, II-10 (in Japanese).

Nordin, C.F. and Rundquist, L.A. (1975) Flume studies with fine and coarse sand, a preliminary analysis. In: *Int. Symp. River Mech.*, Vol. A, pp. 501–511. Bangkok, Thailand.

Rao, K.N., Narashimha, R. and Badri Narayanan, M.A. (1971) The 'bursting' phenomenon in a turbulent boundary layer. *J. Fluid Mech.*, **48**, 339–352.

Raudkivi, A.J. (1963) Study of sediment ripple formation. *ASCE J. Hydraul. Div.*, **89**, 15–33.

Raudkivi, A.J. (1966) Bed forms in alluvial channels. *J. Fluid Mech.*, **26**, 507–514.

Richards, K.J. (1980) The formation of ripples and dunes on an erodible bed. *J. Fluid Mech.*, **99,** 597–618.

Rifai, M.F. and Smith, K.V.H. (1969) Pressure fluctuations in reattaching flow: discussion. *ASCE J. Hydraul. Div.*, **95,** 1747–1750.

Rifai, M.F. and Smith, K.V.H. (1971) Flow over triangular elements simulating dunes. *ASCE J. Hydraul. Div.*, **97,** 963–975.

Robinson, S.K. (1991) Coherent motions in the turbulent boundary layer. *Ann. Rev. Fluid Mech.*, **23,** 601–639.

Rood, K.M. and Hickin, E.J. (1989) Suspended sediment concentration in relation to surface-flow structure in Squamish River estuary, southwestern British Columbia. *Can. J. Earth. Sci.*, **26,** 2172–2176.

Shen, H.W., Fehlman, H.M. and Mendoza, C. (1990) Bed form resistance in open channel flows. *J. Hydraul. Eng.*, **116,** 799–815.

Silveira Neto, A., Grand, D., Métais, O. and Lesieur, M. (1993) A numerical investigation of the coherent vortices in turbulence behind a backward-facing step. *J. Fluid Mech.*, **256,** 1–25.

Simpson, R.L. (1989) Turbulent boundary-layer separation. *Ann. Rev. Fluid Mech.*, **21,** 205–234.

Simons, D.B., Richardson, E.V. and Albertson, M.L. (1961) Flume studies using medium sand (0·45 mm). *U.S. geol. Surv. Water Supply Pap.*, **1498-A,** 76 pp.

Smith, J.D. (1970) Stability of a sand bed subjected to a shear flow of low Froude number. *J. Geophys. Res.*, **75,** 5928–5940.

Smith, J.D. and McLean, S.R. (1977) Spatially averaged flow over a wavy surface. *J. Geophys. Res.*, **82,** 1735–1746.

Soulsby, R.L., Atkins, R., Waters, C.B. and Oliver, N. (1991) Field measurements of suspended sediment over sandwaves. In: *Sand Transport in Rivers, Estuaries and the Sea* (Ed. by R. L. Soulsby and R. Bettess), pp. 155–162. A.A. Balkema, Rotterdam.

Sumer, B.M. and Deigaard, R. (1981) Particle motions near the bottom in turbulent flow in an open channel. Part 2. *J. Fluid Mech.*, **109,** 311–338.

Sumer, B.M. and Ogüz, B. (1978) Particle motions near the bottom in turbulent flow in an open channel. *J. Fluid Mech.*, **86,** 109–127.

Sutherland, A.J. (1967) Proposed mechanism for sediment entrainment by turbulent flows. *J. Geophys. Res.*, **72,** 6183–6194.

Thorne, P.D., Williams, J.J. and Heathershaw, A.D. (1989) *In situ* acoustic measurements of marine gravel threshold and entrainment. *Sedimentology*, **36,** 61–74.

Tritton, D.J. (1988) *Physical Fluid Dynamics*, 2nd edn. Clarendon Press, Oxford, 519 pp.

Van der Knapp, F.C.M., van Mierlo, M.C.L.M. and Officier, M.J. (1991) Measurements and computations of the turbulent flow field above fixed bedforms. In: *Sand Transport in Rivers, Estuaries and the Sea* (Ed. by R. L. Soulsby and R. Bettess), pp. 179–185. A.A. Balkema, Rotterdam.

Van Mierlo, M.C.L.M. and de Ruiter, J.C.C. (1988) Turbulence measurements above artificial dunes. *Rept. TOW A55 Q789*, pp. 1–42. Delft Hydraulics.

Vanoni, V.A. and Hwang, L.-S. (1967) Relation between bed forms and friction in streams. *ASCE J. Hydraul. Div.*, **93,** 121–144.

Vanoni, V.A. and Nomicos, G.N. (1960) Resistance properties of sediment-laden streams. *Trans. Am. Soc. civ. Eng.*, **125,** 1140–1167.

Vittal, N., Ranga Raju, K.G. and Garde, R.J. (1977) Resistance of two dimensional triangular roughness. *J. Hydraul. Res.*, **15,** 19–36.

Wei, T. and Willmarth, W.W. (1991) Examination of *v*-velocity fluctuations in a turbulent channel flow in the context of sediment transport. *J. Fluid Mech.*, **223,** 241–252.

Wiberg, P.L. and Nelson, J.M. (1992) Unidirectional flow over asymmetric and symmetric ripples. *J. Geophys. Res.*, **97,** 12745–12761.

Wiberg, P.L. and Rubin, D.M. (1989) Bed roughness produced by saltating sediment. *J. Geophys. Res.*, **94,** 5011–5016.

Williams, G.P. (1967) Flume experiments on the transport of a coarse sand. *U.S. geol. Surv. Prof. Pap.*, **562–B,** 31 pp.

Williams, J.J. (1990) Video observations of marine gravel transport. *Geo-Mar. Lett.*, **10,** 157–164.

Williams, J.J., Thorne, P.D. and Heathershaw, A.D. (1989) Measurements of turbulence in the benthic boundary layer over a gravel bed. *Sedimentology*, **36,** 956–979.

Willmarth, W.W. & Lu, S.S. (1974) Structure of the Reynolds stress and the occurrence of bursts in the turbulent boundary layer. In: *Turbulent Diffusion in Environmental Pollution* (Ed. by F. N. Frenkiel and R. E. Munn), pp. 287–314. Academic Press, New York.

Yalin, M.S. (1977) *Mechanics of Sediment Transport*, 2nd edn. Pergamon Press, Oxford, 298 pp.

Yalin, M.S. (1992) *River Mechanics*. Pergamon Press, Oxford, 219 pp.

Zippe, H.J. & Graf, W.H. (1983) Turbulent boundary-layer flow over permeable and non-permeable rough surfaces. *J. Hydraul. Res.*, **21,** 51–65.

Manuscript received 29 March 1994; revision accepted 12 August 1994

NOTATION

C_D	bedform drag coefficient
D_{84}	grain size which 84% of the distribution is finer than
f	frequency
f_s	frequency of shear layer fluctuations
Fr	Froude number; $Fr=\bar{U}/\sqrt{gY}$
g	gravitational acceleration
H	threshold (hole size) used in quadrant analysis
h	bedform height

k_S	equivalent sand roughness height
n	number of measurements
Q	quadrant number
S	sorting factor in quadrant analysis
St	Strouhal number
T	burst period
T_b	dimensionless burst period
$\bar{U},\bar{V}$	time-averaged mean downstream and vertical velocity
$\bar{U}_c$	time-averaged mean downstream velocity over crest
U_{skew},V_{skew}	skewness of the velocity distributions
u,v	instantaneous velocity fluctuations about a zero mean
u_i,v_i	instantaneous velocities
u',v'	root-mean-square of the velocity distributions
U_{*B},U_{*SF}	boundary and skin-friction shear velocities
X_r	flow reattachment length
Y	mean flow depth
y	height above the bed
y_0	zero-velocity roughness height
y_*	average internal boundary layer thickness
λ	bedform wavelength
λ_l	wavelength of laser light
κ	von Karman's constant
ρ	fluid density
$\tau_B,\tau_{SF},\tau_{FD}$	boundary, skin-friction and form-drag components of shear stress
τ_r	turbulent Reynolds stress